The discontinuous Galerkin method for river-delta continuum by means of a coupled 1D-2D shallow water model

Insaf Draoui
Ph.D. Student, Institute of mechanics of materials and civil engineering (IMMC), Université catholique de Louvain, Louvain-la-Neuve, Belgium Email: insaf.draoui@uclouvain.be (corresponding author)

Jonathan Lambrechts
Research Associate, Institute of mechanics of materials and civil engineering (IMMC), Université catholique de Louvain, Louvain-la-Neuve, Belgium Email: jonathan.lambrechts@uclouvain.be

Vincent Legat
Professor, Institute of mechanics of materials and civil engineering (IMMC), Université catholique de Louvain, Louvain-la-Neuve, Belgium Email: vincent.legat@uclouvain.be

Eric Deleersnijder
Reader, Institute of mechanics of materials and civil engineering (IMMC) Earth and Life Institute (ELI), Université catholique de Louvain, Louvain-la-Neuve, Belgium Email: eric.deleersnijder@uclouvain.be

ABSTRACT: The 1D Saint-Venant equations are widely used in river modeling for engineering applications. The governing equations maybe formulated in several ways. In discrete form, those formulations are not equivalent. Thus, choosing the convenient intermediate variables for the conservation equations allows optimal stability with minor numerical adjustment. Two different issues should be carefully dealt with in realistic domains: the relative paucity of geometric data and the connection to larger water bodies. Regarding the data interpolation, in the absence of a precise representation of the river bed evolution, we suggest using a general datum for data definition and interpolation along the river, allowing a smooth, stable source term. As for the connection to a 2D model, an implicit boundary-connected coupling based on flux continuity is adopted. The modules above are implemented in the framework of a discontinuous Galerkin finite-element model (SLIM, www.slim-ocean.be). Validation is first performed on idealized configurations. Then, the river-delta continuum of the Mahakam River (Borneo, Indonesia) is modeled, and the results are compared to the measured water level.

1 INTRODUCTION

Free surface flows receive significant attention due to their economic and ecological importance. From the flow in rivers and lakes to the large-scale flow in oceans, the shallow water equations represent an excellent physical way to describe the flow motion. The 3D model may sound the more accurate, but it is time and memory consuming in terms of numerical calculation. Thus simplified 2D depth integrated and 1D section averaged versions are widely used and are known to provide rather reliable results. The integration is made under several assumptions and aims to reduce the number of calculations needed to obtain the approximate numerical solution. The 1D Saint-Venant equations are widely used to represent flow in rivers and channels. But for natural rivers, the model is faced with many challenges (Hodges 2013). We point out mainly the data availability issue. We consider that the solution is approximated using finite element method. In this case the field measurement surveys provide discontinuous geometric data that need to be interpolated on the mesh nodes to recreate the river profile. Many interpolation options are available as presented in Sanders(2004). Polynomial interpolation is widely used for it is easy to implement, with a linear bed evolution between two consecutive field points (Kesserwani 2010). This interpretation of the bed slope might generate many instabilities when dealing with real

rivers. This is why Yu(2020) presents the reference slope method to smooth the source term variation when solving the 1D Saint-Venant equations, using a general reference level along the river.

When dealing with large water bodies or with flood plains the 1D Saint-Venant equations are no longer sufficient. Thus, in the same logic of reducing calculations, it is more optimal to use a different model for each subdomain for some large-scale flows, where we deal with different flow regimes. Here we discuss coupling a simplified 1D model to a more complex 2D one. Those two models can be coupled in many ways; we can distinguish between lateral coupling to deal with flood plains (Kuiry 2010, Marin 2009). It can also be called source term coupling since the 2D input represent a new source term for the 1D model. A river can flow into a lake or an estuary; in this case, the connection is frontal, and the boundary of the two domains are connected (Miglio 2005, Yu 2019). Based on the two systems of equations and the matching conditions, whether the latest is stage conservation, mass and momentum conservation, or flux conservation, the next step is to solve the system of equations. An option is to opt for a simulator coupling. In this case, each sub-model is tackled independently. Then, an external coupling loop is resorted to establish communication between the two models and verify the matching conditions (Chen 2012, Steinebach 2004). The time step of the sub-models might be different. Using an external coupling loop makes efficiency and convergence a critical issue. Another alternative consists in assembling the discrete equations and solving them simultaneously (Neupane 2015, Steinebach 2004). In this case, the conservation of mass and momentum is easily granted since no temporal lag is present for data exchange between the sub-models, but the difficulty is that we end up with a big sparse system to solve; thus, the efficiency of the model is questionable, especially when an explicit scheme is used for temporal integration.

For the coupling scheme we suggest an implicit scheme to solve the coupled system using a discontinuous Galerkin method and a flux based coupling, to give an extra freedom in term of time step choice. As for the data interpolation we build on the reference slope method. We suggest that instead of the linear bed assumption the width data are interpolated parallel to this reference general reference level. In this case the bed slope corresponds to the general slope of the adopted reference level while the width data is seen to pass from zero in a shallow cross-section to a non-zero value in the next deeper cross section. The code is validated over idealized test cases before its application to a real domain.

2 MODEL EQUATIONS

Both 1D Saint-Venant and 2D shallow water equations are conservation equations that take the form :

$$\frac{\partial \mathbf{U}}{\partial t} + \nabla \cdot \mathbf{F}(\mathbf{U}) = \mathbf{S}(\mathbf{U}) \tag{1}$$

where $\mathbf{U}$ is the vector of unknown, $\mathbf{F}(\mathbf{U})$ is the flux of the conserved variables and $\mathbf{S}(\mathbf{U})$ is the source term.

2.1 *1D model*

The 1D Saint-Venant conservation equations adopted is the one detailed in Draoui (2020), with the cross section $A(x,t)$ and the mean discharge $Q(x,t)$ as unknown variables:

$$\mathbf{U} = \begin{pmatrix} A \\ Q \end{pmatrix}, \quad \mathbf{F}(\mathbf{U}) = \begin{pmatrix} Q \\ \dfrac{Q^2}{A} + \dfrac{P}{\rho} \end{pmatrix} \text{ and } \quad \mathbf{S}(\mathbf{U}) = \begin{pmatrix} 0 \\ gA\dfrac{dh}{dx} - gS + \dfrac{F}{\rho} \end{pmatrix} \tag{2}$$

where $P = \rho g \int_0^H (H-z) b \, dz$ is the hydrostatic pressure force exerted on the edge of the control volume; $F = \rho g \displaystyle\int_0^H (H-z)\frac{\partial b}{\partial x} dz$ is the along-flow component of the pressure force resulting from the width variation as shown in Figure 1; $H(x,t)$ is the water depth; $b(x,z)$ is the cross section width at a level z; $\dfrac{dh}{dx}$ is the bed slope and $SA, Q)$ is the friction induced head loss per

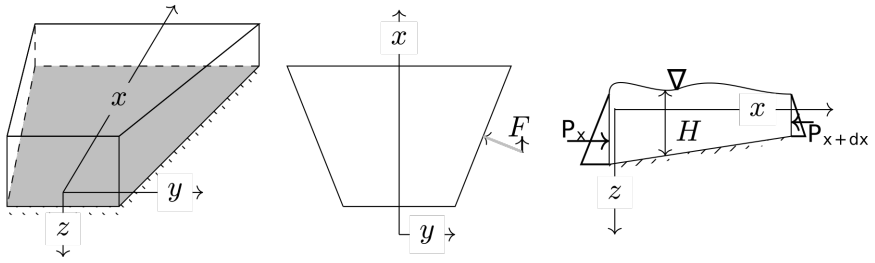

Figure 1. representation of the upstream and downstream pressure force P in the side view (right), a top view of the river (middle) with representation of the lateral pressure induced by width variation, its projection in the x axe represent F.

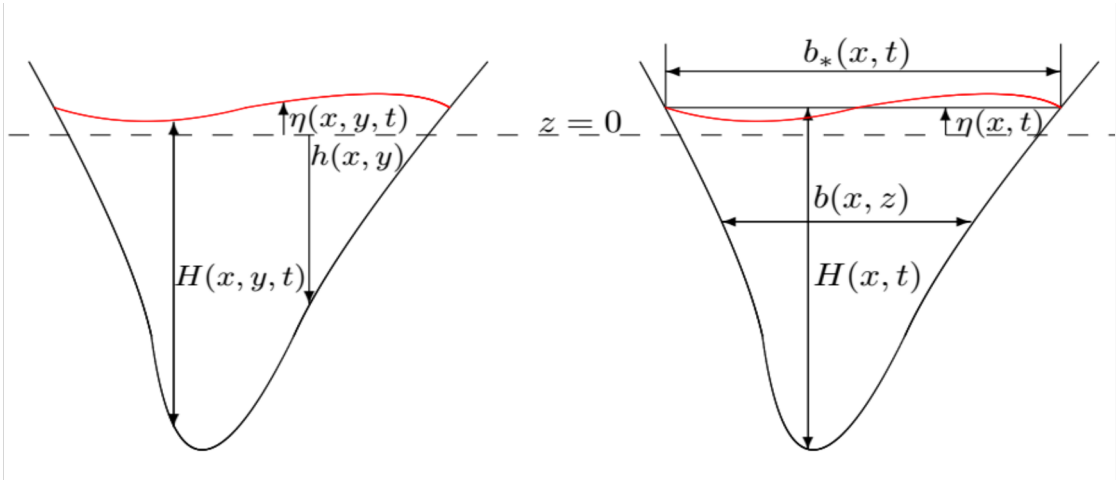

Figure 2. The difference between the 2D and 1D notation in a river cross section. In 1D $\eta(x,t)$ is the mean free surface level, $H(x,t)$ and $h(x)$ are measured to the deepest point. In a 2D model the water depth, water level and bed level are function of both longitudinal coordinate x and transversal one y

unit distance, estimated by means of Manning's formula $S = n^2 \frac{|Q|Q}{AR_h^{4/3}}$ with R_h the hydraulic radius.

2.2 *2D model*

The 2D shallow water equations can be written as Le (2020):

$$\mathbf{U} = \begin{pmatrix} H \\ H\mathbf{u} \end{pmatrix}, \mathbf{F} = \begin{pmatrix} H\mathbf{u} \\ H\mathbf{u}\mathbf{u} + g\frac{H^2}{2} - H\nu\nabla\mathbf{u} \end{pmatrix}, \mathbf{S} = \begin{pmatrix} 0 \\ -\tau_\mathbf{b} + gH\nabla h - f\mathbf{e_z} \times H\mathbf{u} \end{pmatrix} \quad (3)$$

where $\mathbf{u}(u,v)$ is the depth averaged horizontal velocity; μ = the horizontal eddy viscosity; f is the Coriolis parameter; g is the gravitational acceleration and $\tau_\mathbf{b}$ is the bed shear stress. The bed shear stress is estimated by means of Chézy-Manning-Strickler formulation:

$$\tau_\mathbf{b} = \frac{gn^2}{H^{7/3}}|H\mathbf{u}|H\mathbf{u} \quad (4)$$

with n being the Manning coefficient. Figure 2 represents the difference between the 1D and 2D definitions of different flow variables.

2.3 *NUMERICAL METHOD*

In what follows the equations are discretized using a discontinuous Galerkin method. The domain of interest is divided into a set of N elements Ω_e. Inside an element, the variation of variables is approximated using linear shape functions ϕ_i, with $\mathbf{U}_i^e$ the nodal values of the solution:

$$\mathbf{U}|_{\Omega_e} \simeq \mathbf{U}_h|_{\Omega_e} = \sum_{i=1}^{n} \phi_i \mathbf{U}_i^e \quad n \text{ is the number of nodes per element} \tag{5}$$

The conservation laws are multiplied by the test functions and the resulting equations are integrated over each element Ω_e. Applying the divergence theorem the final equation can be written as:

$$\int_{\Omega_e} \frac{\partial \mathbf{U}}{\partial t} \phi_i d\Omega - \int_{\Omega_e} \mathbf{F}.\nabla \phi_i d\Omega + \int_{\Gamma_e} \mathbf{F}\phi_i.\mathbf{n} d\Gamma = \int_{\Omega_e} \mathbf{S}\phi_i d\Omega \tag{6}$$

The flux term $\mathbf{F}.\mathbf{n}$ through the element boundaries Γ_e is replaced by the numerical flux that will be detailed in what follows to take into account discontinuity across the elements edges.

2.3.1 *THE 1D SUBMODEL*

As we integrate the solution over each element apart a discontinuity appears over the elements edges. An element communicates with its neighbour only through the boundary flux $\int_{\Gamma_e} \mathbf{F}\phi_i.\mathbf{n} d\Gamma$. To determine the flux through the discontinuity we define a local Riemann problem. As explained in (Toro 2013) there are many ways to approximate the flux. We adopt a simple approximate-state solution. As detailed in Draoui (2020), the conservation equation (1) is locally linearized using the mean nodal value of both sides of the element edge. The Riemann invariants are used to evaluate the star variables; corresponding to the solution in the wedge between the two characteristics of the problem. The unicity of the solution derives from the flux and energy conservation; $Q_e^* = Q_{e+1}^*$ and $A_e^* = A_{e+1}^*$:

$$\begin{cases} \text{On } \Omega_e \quad A^* \left(-\dfrac{Q_0}{A_0} + \sqrt{\dfrac{gA_0}{b^*}} \right) + Q^* = A_e \left(-\dfrac{Q_0}{A_0} + \sqrt{\dfrac{gA_0}{b^*}} \right) + Q_e \\ \text{On } \Omega_{e+1} \quad A^* \left(\dfrac{Q_0}{A_0} + \sqrt{\dfrac{gA_0}{b^*}} \right) - Q^* = A_{e+1} \left(\dfrac{Q_0}{A_0} + \sqrt{\dfrac{gA_0}{b^*}} \right) - Q_{e+1} \end{cases} \tag{7}$$

Finally the flux is calculated based on the star variables as $\mathbf{F}(\mathbf{U}^*)\phi_i$.

2.3.2 *THE 2D SUBMODEL*

The Lax-Friedrichs flux is adopted for the 2D model (Nair 2005,Toro 2013). The numerical flux at the interface between element Ω_e and Ω_{e+1} corresponds to the mean value of $\mathbf{F}(\mathbf{U})$ to which we apply a correction that aims to smooth the discontinuity at the edge. This correction corresponds to the solution jump $\mathbf{U_{e+1}} - \mathbf{U_e}$ that would be traveling at the maximum wave speed. $c = \max(\sqrt{gH_e}, \sqrt{gH_{e+1}})$:

$$\tilde{\mathbf{F}} \cdot \mathbf{n} = \frac{1}{2} \Big[(\mathbf{F}(\mathbf{U}_e) + \mathbf{F}(\mathbf{U}_{e+1})) \cdot \mathbf{n} - c(\mathbf{U}_{e+1} - \mathbf{U}_e) \Big] \tag{8}$$

The Lax-Friedrichs is suitable for advection problems. Thus the diffusive term $\nu H \nabla \boldsymbol{u}$ should be dealt with separately. We implement an incomplete interior penalty method (Rivière 2008). In this case, in addition to the mean value of the diffusive flux we apply the following correction:

$$\widetilde{\nu H \nabla} \mathbf{u}.\mathbf{n} = \frac{\nu}{2} \left((H_e \nabla \mathbf{u_e} + H_{e+1} \nabla \mathbf{u_{e+1}}).\mathbf{n} - \sigma \frac{H_e + H_{e+1}}{2} (\mathbf{u_{e+1}} - \mathbf{u_e}) \right) \tag{9}$$

with σ a penalization parameter defined as:

$$\sigma = \frac{(p+1) * (p+2)}{2} \frac{\text{edge length}}{\text{element area}} \tag{10}$$

with p the polynomial order of the finite element space equal to one for we are adopting a linear DG, and the fraction length by area is taking as the maximum value between adjacent elements (Shahbazi 2005).

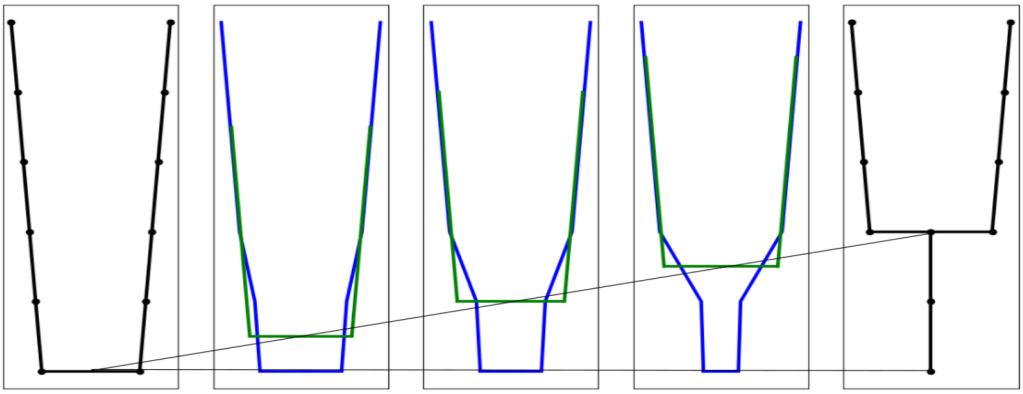

Figure 3. Width interpolation at three intermediate points, based on two input data $-\bullet-$, the green sections $-$ correspond to a linear interpolation parallel to the linear bed and the blue section $-$ correspond to a linear interpolation parallel to a horizontal level.

2.4 *BOUNDARY CONDITIONS*

For a boundary node in a 1D domain or a boundary edge for the 2D model we need also to evaluate the numerical flux as for the internal nodes (edges). As we are dealing with subcritical flow a characteristic is leaving the domain boundary while another one is entering it. In this case a Riemann invariant can be determined from internal values while the other one requests an external value (Guinot 2012). Thus only one external value of our state variables must be given at a boundary while the other one is copied for the internal cell. As we have now both side values of our variable $\boldsymbol{U}$ at our boundary, the numerical flux is estimated in the same way us was presented earlier for an internal cell boundary.

2.5 *COUPLED 1D/2D BOUNDARY*

Let us consider the interface between the 2D domain and 1D domain. The two models solve different state variables. In the 2D model the flow direction is described using the velocity vector, while in the 1D domain, the flow has only one direction that corresponds to the edge mesh cell direction. We consider a flux-based connection (Bladé 2012), but with an implicit temporal scheme. The 2D numerical flux is given to the 1D model. To evaluate this flux, we need to provide the H_{1d} and $\mathbf{u}_{1d}$, based on the 1D boundary. At the 2D boundary edge, the bed level is defined in reference to $\eta = 0$. In this case when the real water level is greater than zero, we assume that the 2D cross section is extended by walls at the edge with the same width as the edge length w_c itself. Thus from the 1D cross section H_{2d} is evaluated as:

$$H_{2D}(x, y, t) = \frac{(A_{1D} - A_{2D}|_{\eta=0})}{w_c} + h(x, y, t) \tag{11}$$

On the other hand, the transport is directly approximated by dividing the 1D volumetric flow rate Q_{1D} by w_c. The obtained transport is normal to the boundary edge and should be projected on the x and y axes. The rest of the calculation is done as was explained for each model separately then the systems are assembled in a spare linear matrix for an optimal use of memory.

3 GEOMETRY DATA INTERPRETATION AND INTERPOLATION

The issue of data interpretation is mainly present in the 1D model. From the surveys or the satellite image analyses, we end up with a set of points that we connect to build the river cross-section at different locations. For an optimal fit of a natural cross-section, the latter is seen as a succession of trapezoids. The width data are then stored per vertical level and used to evaluate the pressure forces and the cross-section at different levels. Next, we interpolate those data on the mesh nodes first and on the integration points during the simulation. Using a first-order discontinuous Galerkin method, the interpolation on the integration points is linear. On the other hand, the interpolation on the mesh nodes can be of a higher order for a better representation of the geometry. The

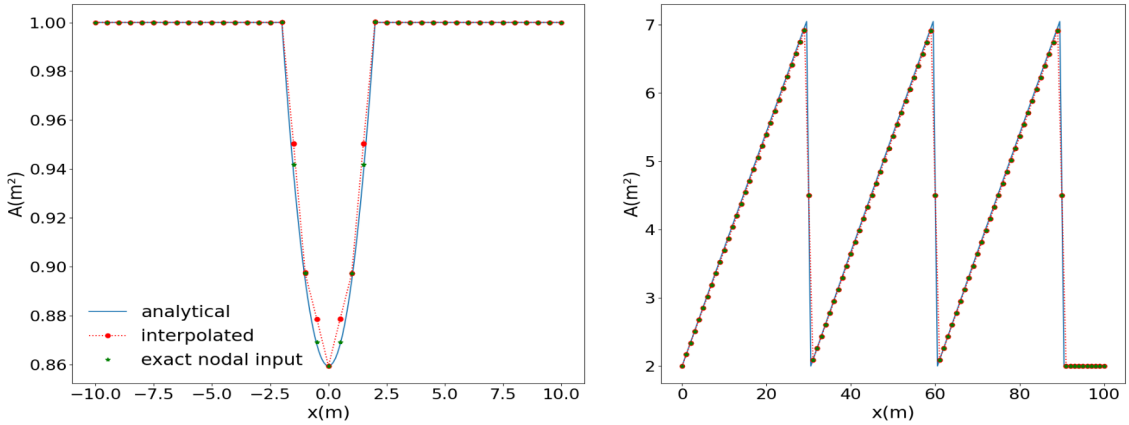

Figure 4. Exact analytical cross-section and numerical results using discrete inputs and exact nodal inputs for subcritical flow over a hump (left) and subcritical sudden contraction (right).

question is how the bed level develops between two consecutive cross-sections. If we assume a linear variation of the bed which might seem quite natural, we face a numerical issue related to the non-smooth source term. As bed level variation appears as a source term of the momentum equation and as explained in (Yu 2019) a non-smooth source term creates instabilities. We build on the article's suggestion of using a general datum for a reference slope that would be a mean value along the river. We suggest extending the global datum and using it for width interpolation. In this case, the depth between two consecutive cross-sections is constant; a zero width value extends a shallow cross-section. As depicted in Figure 3 if we consider a simple trapezoidal cross-section, we suggest that the interpolation is made parallel to a global datum. Hence the slope source term corresponds to the mean slope of the datum.

4 VALIDATION TEST CASES

In the idealized test cases the temporal term $\partial \mathbf{U}/\partial t$ is integrated using an implicit Euler scheme. We consider two idealized steady flows over friction-less rectangular $1m$ wide channel. In absence of friction induced head loss the analytical solution is built based on Bernoulli equation for energy conservation:

$$H(0) + h(0) + \frac{Q^2}{2gH(0)} = H(x) + h(x) + \frac{Q^2}{2gH(x)} \tag{12}$$

To test the interpolation method introduced earlier we consider a horizontal datum ($dh/dx = 0$). We solve the test cases in two different ways. In one case we define discrete input points with the correct width and cross section that we interpolate later linearly on the mesh nodes. In the other case we give the exact width and cross section values per mesh nodes. In both cases the nodal mesh inputs are linearly interpolated on the integration points.

Subcritical sudden contractions:

As detailed in Murillo(2014), we consider a $100m$ length channel with a variable bed. The upstream discharge is $2m^3/s$ and the downstream water level is $2m$. We consider a horizontal datum for data interpolation, for a mesh size of $dx = 1m$. The discrete input nodes corresponds to the x coordinates $[0, 10, 20, 29.5, 30.5, 40, 50, 59.5, 60.5, 70, 80, 89.5, 90.5, 95, 100]$.

Subcritical flow over a bump:

We consider a $20m$ length channel with a bed level $h(x) = \max 0, 0.1(1 - 0.25x^2)$. The upstream discharge is $1.5m^3/s$ and the downstream water level is $1m$. We consider a horizontal datum for data interpolation, for a mesh size of $dx = 1m$. The discrete input nodes corresponds to the a horizontal step of $0.5m$. The obtained results are depicted in Figure 4. In both idealized cases, the numerical solution is close to the analytical one. The Root mean square error for the interpolated data and correct nodal input are respectively 0.0037 and $0.0015m^2$, while for the sudden contraction the bed itself being linear the error of both methods is identical for both inputs with a vale of $0.83m^2$. Regarding quadratic bed evolution in the flow over a bump a

quadratic interpolation over the mesh nodes might provide more accurate nodal data to improve the numerical result.

Application to the Mahakam river:

The Mahakam river flows in Indonesia, from Borneo's central mountain to the east south of the island, where it discharges into the Makassar Strait. The geometric data used for the simulation are obtained from fieldwork campaigns in 2008 and 2009 (Sassi 2011). The data spacing is 100m. The 1D river model is connected to a 2D model that represent the Mahakam delta and a part of the Makassar strait. At the open ocean the tidal elevations and velocity are provided from OSU TOPEX/Poseidon Global Inverse Solution. The upstream boundary condition at river branches are those of Sassi (2011). For the period between 12-06-2008 to 01-07-2008 we compare the obtained results to field measurement in one point of the 1D domain near the delta apex and an other point in the north part of the delta as depicted in Figure 5. We observe a good agreement between simulated water levels and measured ones.

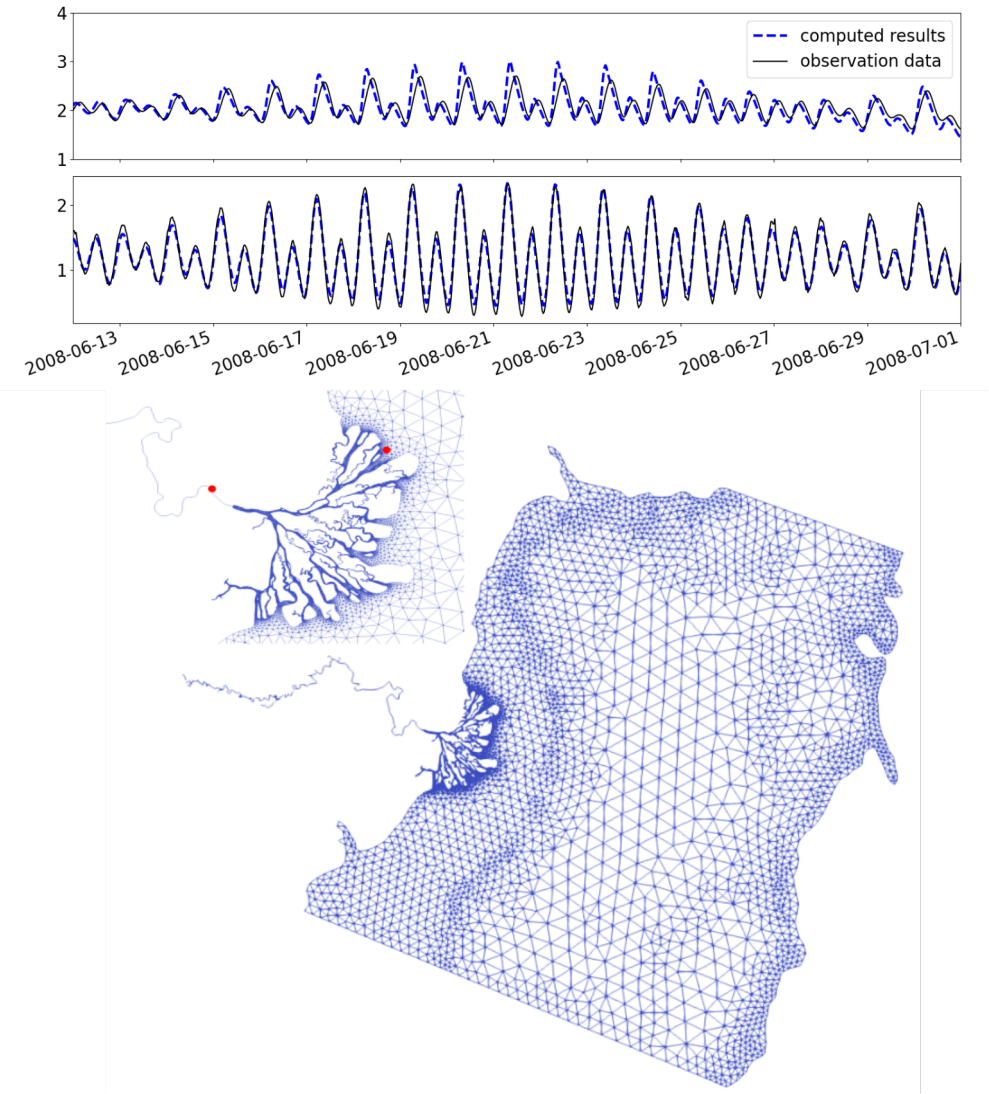

Figure 5. Plot of the measured and simulated water level evolution over time in the 1D station (top upper panel) and the 2D station. the • in the mesh represent the location of the measurement stations. The Manning coefficient for the river ans sea are respectively 0.03 and 0.025 $sm^{-1/3}$.

5 DISCUSSION AND CONCLUSION

This paper presents a discretization of the 1D and 2D shallow water equations using an implicit first order discontinuous Galerkin method. We underscore the importance of the data interpolation in the 1D model that might reduce the numerical stabilization needed for the source term simply by giving a different interpretation to the bed evolution. When connected to the 2D model, the flux coupling proved its performance in reproducing the reality. The implicit temporal integration allow more freedom in time step choice. Using explicit temporal scheme, with the small elements in the delta, we can not exceed a time step of $.1s$, while the time step used for the implicit simulation is $900s$.

REFERENCES

Bladé, E., Gómez-Valentín, M., Dolz, J., Aragón-Hernández, J. L., Corestein, G., & Sánchez-Juny, M. (2012). Integration of 1D and 2D finite volume schemes for computations of water flow in natural channels. Advances in Water Resources, 42, 17-29.

Chen, Y., Wang, Z., Liu, Z., & Zhu, D. (2012). 1D–2D coupled numerical model for shallow-water flows. Journal of hydraulic engineering, 138(2), 122-132.

Draoui, I., Lambrechts, J., Legat, V., Soares-Frazao, S., Hoitink, T., & Deleersnijder, E. (2020). Discontinuous Galerkin method for 1D river flows. In River Flow 2020 (pp. 1114-1121). CRC Press.

Guinot, V. (2012). Wave propagation in fluids: models and numerical techniques. John Wiley & Sons.

Hodges, B. R. (2013). Challenges in continental river dynamics. Environmental modelling & software, 50, 16-20.

Kesserwani, G., Liang, Q., Vazquez, J., & Mosé, R. (2010). Well-balancing issues related to the RKDG2 scheme for the shallow water equations. International journal for numerical methods in fluids, 62(4), 428-448.

Kuiry, S. N., Sen, D., & Bates, P. D. (2010). Coupled 1D–Quasi-2D flood inundation model with unstructured grids. Journal of Hydraulic Engineering, 136(8), 493-506.

Le, H. A., Lambrechts, J., Ortleb, S., Gratiot, N., Deleersnijder, E., & Soares-Frazão, S. (2020). An implicit wetting–drying algorithm for the discontinuous Galerkin method: application to the Tonle Sap, Mekong River Basin. Environmental Fluid Mechanics, 20(4), 923-951.

Sanders, B. F., & Chrysikopoulos, C. V. (2004). Longitudinal interpolation of parameters characterizing channel geometry by piece-wise polynomial and universal kriging methods: effect on flow modeling. Advances in water resources, 27(11), 1061-1073.

Marin, J., & Monnier, J. (2009). Superposition of local zoom models and simultaneous calibration for 1D–2D shallow water flows. Mathematics and Computers in Simulation, 80(3), 547-560.

Miglio, E., Perotto, S., & Saleri, F. (2005). Model coupling techniques for free-surface flow problems: Part I. Nonlinear Analysis: Theory, Methods & Applications, 63(5-7), e1885-e1896.

Murillo, J., & García-Navarro, P. (2014). Accurate numerical modeling of 1D flow in channels with arbitrary shape. Application of the energy balanced property. Journal of computational Physics, 260, 222-248.

Nair, R. D., Thomas, S. J., & Loft, R. D. (2005). A discontinuous Galerkin global shallow water model. Monthly weather review, 133(4), 876-888.

Neupane, P., & Dawson, C. (2015). A discontinuous Galerkin method for modeling flow in networks of channels. Advances in Water Resources, 79, 61-79.

Rivière, B. (2008). Discontinuous Galerkin methods for solving elliptic and parabolic equations: theory and implementation. Society for Industrial and Applied Mathematics.

Sassi, M. G., Hoitink, A. J. F., De Brye, B., Vermeulen, B., & Deleersnijder, E. (2011). Tidal impact on the division of river discharge over distributary channels in the Mahakam Delta. Ocean Dynamics, 61(12), 2211-2228.

Shahbazi, K. (2005). An explicit expression for the penalty parameter of the interior penalty method. Journal of Computational Physics, 205(2), 401-407.

Steinebach, G., Rademacher, S., Rentrop, P., & Schulz, M. (2004). Mechanisms of coupling in river flow simulation systems. Journal of Computational and Applied Mathematics, 168(1-2), 459-470.

Toro, E. F. (2013). Riemann solvers and numerical methods for fluid dynamics: a practical introduction. Springer Science & Business Media.

Yu, C. W., Hodges, B. R., & Liu, F. (2020). A new form of the Saint-Venant equations for variable topography. Hydrology and Earth System Sciences, 24(8), 4001-4024.

Yu, K., Chen, Y., Zhu, D., Variano, E. A., & Lin, J. (2019). Development and performance of a 1D–2D coupled shallow water model for large river and lake networks. Journal of Hydraulic Research, 57(6), 852-865.